

STRUCTURAL INTEGRITY AND MATERIALS AGEING IN EXTREME CONDITIONS

S.T. Tu
Z.D. Wang
G.C. Sih

EAST CHINA UNIVERSITY OF SCIENCE AND TECHNOLOGY PRESS



012015151

Copyright and Reprint Permission: All right are reserved. No part of this publication may be reproduced, stored in as retrieval system, or transmitted in any means, electronic, mechanical, photo-copying or otherwise, without the prior permission of East China University of Science and Technology Press and Editors, S.T. Tu, Z.D. Wang and G.C. Sih. The chapters are reproduced with permission from the individual authors.

Copyright © 2010 East China University of Science and Technology Press, and S.T. Tu, Z.D. Wang and G.C. Sih.

East China University of Science and Technology Press

Shanghai 200237, China

图书在版编目 (CIP) 数据

极端条件下结构完整性与材料老化: 英文/涂善东, 王正东, 薛昌明 编著

——上海: 华东理工大学出版社, 2010.10

ISBN 978-7-5628-2906-5

I. ①极... II. ①涂... ②王... ③薛... III. ①断裂力学—国际学术会议—文集—英语 IV. ①0346.1-53

中国版本图书馆 CIP 数据核字 (2010) 第 192960 号

极端条件下的结构完整性与材料老化

Structural Integrity and Materials Ageing in Extreme Conditions

编 著/涂善东 王正东 薛昌明

责任编辑/徐知今

责任校对/金慧娟 张波

封面设计/陆丽君

出版发行/华东理工大学出版社

社 址: 上海市梅陇路 130 号, 200237

电 话: (021) 64250306 (营销部)

传 真: (021) 64252707

网 址: Press.ecust.edu.cn

印 刷/江苏句容市排印厂

开 本/787mm×1092mm 1/16

印 张/27.5

字 数/936 千字

版 次/2010 年 10 月第 1 版

印 次/2010 年 10 月第 1 次

印 数/1-700 册

书 号/ISBN 978-7-5628-2906-5/TB·37

定 价/150 元

(本书如有印装质量问题, 请到出版社营销部调换。)

Preface

This book presents the proceedings of the international symposium on structural integrity (ISSI), held in Shanghai on October 21-24, 2010. As the successor of Fracture Mechanics symposium series (from 2003 to 2009), ISSI is devoted to the exchange of information among the universities, research institutions and industry sectors in China and abroad. The first symposium on structural integrity (FM2003) was held in 2003 at East China University of Science and Technology, Shanghai. Since then, annual meetings have taken place at different cities in China. This includes FM2004 in Huangshan, Anhui Province, FM2005 in Zhengzhou, Henan Province, FM2006 in Nanjing, Jiangsu Province, FM2007 in Changsha, Hunan Province, FM2008 in Hangzhou, Zhejiang Province and FM2009 in Chengdu, Sichuan Province. The symposium series has played an important role in promoting information exchange, inspiring new ideas, integrating practical and research findings and breaking new grounds for the young generation. In particular, it accelerates the birth of China Structural Integrity Consortium and promotes the development of structural integrity technology in the country.

With the increased demand for higher efficiency and reduced emission, the working conditions of machines have been going extreme. To ensure the safe operation of the machines, the structural integrity technology plays a key role in materials selection and product design, manufacture and maintenance. In addition, the size of engineering components can vary from nanometers to very large scale of thousands meters. The new developments of high techs, such as high power electronics, MEMS, MCMS (micro chemo-mechanical systems) and mega engineering structures provide additional challenges to structural integrity. To meet the challenges of extreme working conditions and structural sizes, the failure mechanisms of the components or machines should be studied, existing theories of structural integrity should be reexamined and new theories be developed. Innovations in materials and structural design are the basis to ensure the structural safety which should be of high priority in research. Structural integrity prognosis or structural health monitoring provides an important solution to structural safety which may need more R&D efforts. Aiming at bridging the gap between new challenge and fundamental researches, ISSI2010 brings together the scientific community and the engineering community to exchange their new developments and ideas for structural integrity assessment.

The symposium (ISSI2010) is co-organized by East China University of Science and Technology, National Engineering Research Center of Pressure Vessels and Pipelines Safety Technology (General Machinery Research Institute), Energy Safety Research Institute of Chung Ang University, Nanjing University of Technology, Zhejiang University, Zhejiang University of Technology, Zhengzhou University, Changsha University of Science and Technology, Shandong University, Southwest Jiaotong University and Beihang University, and co-sponsored by China Structural Integrity Consortium, Korean Society of Mechanical Engineers (Fracture and Strength Division), Natural Science Foundation of China, General Administration of Quality Supervision, Inspection and Quarantine of China.

On behalf of the organizing committee, we would like to thank the above co-organizers and co-sponsors who made ISSI2010 possible. We also appreciate the efforts of the steering committee members in reviewing and selecting the papers. We are indebted to Professor George C. Sih and Professor Zhengdong Wang for their passion to the symposium and efforts made to ensure the success of the event.

Fu-Zhen Xuan
Executive Chairman
East China University of Science & Technology

Shan-Tung Tu
Symposium Series Chairman
East China University of Science & Technology

October, 2010

Contents

Preface

Greener and higher energy efficiency for materials and structural systems sustaining against aggressive environment G. C. Sih	1
Consideration of material aging properties in longer-term failure predictions of cracked components Kamran Nikbin	15
Coupling effect of creep deformation and internal stress on scale growth under the applied bending Fu-Zhen Xuan, Qing-Qi Chen, Shan-Tung Tu	17
Residual stresses in welded nuclear power components D. J. Smith	27
Current research topics for nondestructive reliability evaluation in NIMS Makoto Watanabe, Dongfeng He, Hisashi Yamawaki, Mitsuharu Shiwa	37
Relaxation of residual stresses and grain boundary fracture in 316H stainless steel P. E. J. Flewitt, B. Chen, D. J. Smith	41
Effects of service cycles on the microstructure and tensile property of K4648 superalloy Zhipeng Li, Sujun Wu, Sheng Zhang, Ying Liu	51
Characterization of mechanical properties of HP40Nb using indentation creep test Weize Wang, Bo Wang, Fu-Zhen Xuan, Zhengdong Wang, Changjun Liu	57
Experimental study on the mechanical properties of H13-TiC composite coatings Yifang Hou, Shengting Gu, Yumei Bao, Guozhong Chai	61
Experimental study on creep-ratcheting-fatigue interaction of SS304 stainless steel at room and high temperatures Juan Zhang, Guozheng Kang, Qing Gao, Yujie Liu	67
High-temperature corrosion-resistance property of Fe-Al/Cr ₃ C ₂ RE composite coatings produced by HVFS Xiaoming Liu, Junhui Dong, Runsheng Xu	73
Comparison of ductile-to-brittle transition curve fitting approaches L. W. Cao, S. J. Wu, P. E. J. Flewitt	79
Microstructure and intergranular corrosion of 316L stainless steel diffusion bonded joint Lei Li, Shu-Xin Li, Shu-Rong Yu, Hong-Bo Xia	85
Accelerated pitting corrosion of welded SUS304 under freezing and thawing corrosive environment	

Kazunori Ishitsuka, Junichi Shibano, Tsuyoshi Takahashi, Setsuo Miura, Michiaki Kobayashi	91
Bending fretting fatigue damages of 316L austenitic stainless steel plates against 52100 steel cylinders J. F. Peng, C. Song, M. X. Shen, J. Luo, C. S. Jiang, M. H. Zhu	97
Stress corrosion crack study of 304 and 316L stainless steel in dye solution Zhiming Lu, Shuiping Sheng, Chenghui Zhu, Longjuan Zhang	101
Corrosion resistance of 321 stainless steel in high-temperature naphthenic acid Ke Jiang, Tiecheng Yang, Xuedong Chen, Zengliang Gao	105
Research on anisotropy properties of A350 pressure vessel steel forging by small punch test Ming Song, Kaishu Guan, Lixun Zhao, Zhiwen Wang	111
Prediction methodology of stress relaxation performance based on continuum damage mechanics Jinquan Guo, Fu-Zhen Xuan, Zhengdong Wang, Shan-Tung Tu	117
Strengthened with carbon fiber sheets and its implementation Xiaoyan Liu, Cuiping Tang, Weiqing Zhu	121
Failure analysis of 20G boiler tubes Hudong Liu, Weiqiang Wang, Mengli Li, Shugen Xu, Haoxuan Cui	127
A study on the plasma treatment effect carbon fibers on the wear properties of carbon/epoxy woven composites Jae-Seok Lee, Bong-Hyun Lee, Kyong-Yop Rhee	133
Relationship between elevated strength and brazing parameters of Inconel Superalloy vacuum brazed joints Chunwei Ma, Kun Shi, Zhishui Yu, Peiquan Xu	137
Temperature rise rate of steam turbine at cold-state start-up considering the hardness changes of rotor materials Pinghua Yang, Jiming Yang, Jian Chen, Jianjun He, Wei Qiu, Yanjie Ren, Jianlin Chen	141
Effect of solid solution treatment on microstructure and properties of 0Cr18Ni9 Austenite stainless steel butt-welding pipe fittings Tao Chen, Xuedong Chen, Zhibin Ai, Xiaoming Lian	147
The influence of tensile stress on the magnetic memory signals of Q345R steel Pengju Guo, Xuedong Chen, Weihe Guan, Huayun Cheng, Heng Jiang	153
Fracture mechanism of low cycle fatigue of 30Cr1Mo1V steel at different loading rates Jianjun He, Jian Chen, Qingmin Sun, Jianlin Chen, Pengzhan Zhou	157
Determination of mode I fracture toughness, G_{IC} , of dispersion improved clay/epoxy nanocomposites Sang-Hoon Kim, Man-Tae Kim, Sung-Rok Ha, Kyong-Yop Rhee	163
Analysis of fracture property for beam-column connections of steel frame with cracks Yuping Sun, Yi Li	167

Free vibration analysis of thin rectangular cracked plate with four free edges on nonlinear elastic foundation Guanglin Feng, Cuiping Yang, Yonggang Xiao	173
Failure mechanism of inconel 718 at elevated temperature Nu Yan, Norio Kawagoishi, Li Li	179
Damage tolerance assessment and test verification for an aeroengine crankcase Liye Qin, Sujun Wu, Haitao Zhao, Ying Liu	183
Thermal damage of cementitious materials: an elasto-plastic damage model for plain concrete subjected to high temperatures A. Menou, Gh. Mounajed, H. Boussa, Ch. La Borderie, A. Saouab	189
Two-step damage identification approach for a multi-layer concrete frame structure based on wavelet analysis and BP neural network Xuhua Deng, Xuesong Tang	199
3-D numerical of simulation of concrete failure process based on dynamic damage Shangzhi Zhou, Xiaoping Guo, Shengcai Xiao	205
Quantitative characterization and analysis of creep constraint induced by specimen thicknesses in compact tension specimens Pengjuan Sun, Guozhen Wang, Fu-Zhen Xuan, Shan-Tung Tu, Zhengdong Wang	213
Experimental study on residual fatigue life for a nickel-based powder metallurgy superalloy Bin Zhong, Xinyue Huang, Weibin Guo, Huichen Yu	221
Fatigue crack growth behavior in stainless steel under cyclic torsion Huichen Yu, Keisuke Tanaka	227
A numerical method to simulate ductile failure of tensile plates with interacting through-wall cracks Nak-Hyun Kim, Chang-Sik Oh, Yun-Jae Kim	233
Numerical simulation of crack propagation and coalescence in plates under creep conditions Jian-Feng Wen, Shan-Tung Tu, Fu-Zhen Xuan	247
Research on effect of anti-vibration bars on dynamic characteristic of U-tubes in steam generator Qiwu Dong, Ke Wang, Suzhen Wang, Xin Gu, Tong Liu	257
Fatigue-cracking representation and its evolution for spherical contacts Jianhua Xiao	261
Prediction of creep life in terms of dissipated power Hui Liu, Fu-Zhen Xuan, Guoping Xu	269
Study on limit load and safety assessment method for pressure pipe with an internal pit at high temperature Xiaohua He, Jianwen Sheng, Bo Wang, Jilin Xue, Changyu Zhou	275
Evaluating residual stress behaviour in 316H stainless steel using neutron diffraction	

B. Chen, D. J. Smith, P. E. J. Flewitt, S. Y. Zhang	281
Limit loads for part-through surface axially cracked elbows under internal pressure Chen Wang, Yinpei Wang, Peining Li, Jin Chen, Xiaoming Sun	287
Safety assessment of pipes with multiple local wall thinning defects under bending moment Jian Peng, Changyu Zhou, Jilin Xue, Qiao Dai	293
Effect of the applied torque on the PEM fuel cell performance Yanchao Xin, Jinzhu Tan, Y. J. Chao	299
Contact resistance and contact behavior prediction between the bipolar plate and the GDL in a proton exchange membrane fuel cell Guo Li, Jinzhu Tan, Jianming Gong	305
A new form of strain gradient elasticity Bing Zhao, Yingren Zheng, Xiaoqiang Yan, Jialin Hou	311
Structure strength and safety analysis of CO ₂ stripper with large opening under vertical position Peng Wang, Jianping Zhao	317
Reinforcement of pressure vessels with large opening Minshan Liu, Lina Mei, Qiwu Dong	323
Finite element analysis on welding residual stresses of T-joint Yuping Sun, Junbo Yan	329
Finite element analysis on the contact stress of automotive water pump bearing's seal Qiong Zhou, Zhengmei Li, Jianping Tang, Zemin Xu, Qi An	335
Numerical investigating the effect of braze processing parameters on residual stresses in an X-type lattice truss sandwich structure Wenchun Jiang, Jianming Gong, Shan-Tung Tu	341
Numerical simulation of electromigration failure in IC interconnect structures Yuanxiang Zhang, Yong Liu, Lihua Liang	349
Numerical simulation and structure optimization of coal-liquefying reactor Yihao Wang, Shaoping Zhou, Geling Yang, Jianhua Lan	356
FEA analyses under tension and bending fretting fatigue modes C. Song, J. F. Peng, M. X. Shen, C. S. Jiang, M. H. Zhu	363
Finite element stress analysis of semi-trailer liquefied petroleum gas tanker Jianhua Pan, Xuedong Chen, Zuoquan Yao, Zongchuan Qin, Hui Feng Jiang	365
Analysis of uneven settlement effects on the widened bridge Minshan Liu, Qing Cai, Qiwu Dong, Qiongshu Su	369
Identification of structural parameters by the weighted least square method based on wavelet packet transform	

Yichun Ren, Weijian Yi	373
Study on the non-probabilistic interval reliability of pressure pipe containing defects Linfeng Pan, Changyu Zhou	379
A new DEM for interaction between adjacent RC membrane structures S. B. Cai, B. A. Izzuddin, A. Elghazouli, P Shen	385
A new method for assessment of spurious trip in safety instrumented system Zhenyu Ding, Shiyi Bao, Zengliang Gao	393
On-line monitoring of high-temperature piping by strain sensing units Ning Wang, Xiaoyin Hu, Jiuhong Jia, Zhengdong Wang, Shan-Tung Tu	399
Simulation of inclusion shape change in steel strips during cold rolling Yuxi Yan, Ming Zhang, Hongliang Pan	405
A method of assessing power-law creep constants using small punch creep test in high temperature components Kee Bong Yoon, Young Wha Ma	411
Ratcheting analysis of pressurized piping with pit defects Qi Zhang, Dunji Yu, Zhen Xu, Xu Chen	417
Author index	423
Keywords index	425

Greener and higher energy efficiency for materials and structural systems sustaining against aggressive environment

G. C. Sih *

*International Center of Sustainability, Accountability and Eco-Affordability of Large Structure (ICSAEELS), Lehigh University,
Bethlehem PA 18015, USA*

School of Mechanical Engineering, East China University of Science and Technology, Shanghai 200237, China

Abstract

Shortened technology adoption rate has been exerting relentless pressure on adopting total reliability to multi-component structural systems for preventing the destruction of the whole from the failure of a single part. High reliability is tenable for operation without failure by invoking corrective measures from the monitored in-situ data. To this end, multi-subroutines of large scale computational algorithms should possess open system thermodynamic characteristics such that the simulation is indeed compatible with the monitored in-situ data in open environments. Energy dissipation, non-homogeneity non-equilibrium, cumulative damage, etc., are just some of the features that should be considered in the modeling of the structural degradation process. These multifaceted requirements disqualifies long term predictions beyond 2 to 3 years. Each subroutine is designed to satisfy an aspect of the multifunctional system behavior. The overall program can simulate strong and weak reliability depending on the definition of the reliability time limit. The subroutines can be arranged for the components to fail one at a time in sequence until a set time. The system can also be terminate when only one part would fail. Different scenarios with varying causes and effects of failure can be accommodated. The combined use of monitored in-situ data with quick feed back for corrective measures allows short term deterministic prediction. This overall scheme is referred to loosely as “total reliability”.

Keywords: Total reliability; Green energy; Efficiency; Multiscale; Multifaceted criteria; Multifunctional systems; Design flexibility; In-situ data; Common base of evaluation.

1. Introduction

The continue contamination of the environment from excessive emission of GHG has been a global concern, a natural phenomenon caused by over population of the human habitat. Escalation of the natural resources has been identified with the rapid depletion of useful energy that is being converted into carbon dioxides and other gases. This effect is further aggravated by climate changes and referred to as GHG emission. It is now a recognized fact that unbalance of the ecological cycle must be and can be mitigated by enhancing the thermodynamic efficiency of the energy consumed for all sectors of the societal infrastructures. This may include air, land and sea transports, tall buildings, bridges, energy generation power plants, and others. The average efficiency range of energy consuming sys-

tems is hovering around 30% to 40% [1], simply because energy efficiency has not been regarded as a primary design criterion. A consulted effort would require a common base for assessing the efficiency of the energy consumed by diversified physical systems [2, 3]. Energy efficiency should be focused on the intensity of energy entrapped in contrast to that dissipated within a fixed volume of material. This places precedent on “energy density” rather than energy. What really counts is the time rate of energy density consumption. *Power density efficiency* [4, 5] would be the proper ranking parameter, the use of which would require fundamental changes in the physical meaning of the intrinsic energy dissipated. One of these changes is the simultaneous occurrence of dissipation energy density \mathcal{D} with absorption energy density \mathcal{A} . The former cannot prevail without the latter. The measurement of energy efficiency, in fact, depends on the ratio of \mathcal{D}/\mathcal{A} , not \mathcal{D} or \mathcal{A} alone. This interpretation has been demonstrated for the Being jet transports in the past and the recent Boeing 787-9 whose energy effi-

* Corresponding author.

E-mail address: gcs@ecust.edu.cn; zpg7463@yahoo.com (G. C. Sih).

ciency can be as high as 50% or more as compared with vintage version of the Boeing 757s whose efficiencies are about 30%. These improvements are being made possible by the use of multi-component and multiscale structures [6, 7]. Multiscale does not only refer to components of different sizes, but the more important implication is that *the physical mechanisms and laws governing the material internal structure change when the size is changed*. Small bodies do not obey the same physical laws as those for the larger bodies [4, 5]. The mal-function of a minute electronic device can lead to major disaster as a result of the failure of a critical structural component. Such disasters have been occurring more and more frequently. System reliability [8] has thus been a real concern.

Multi-component systems are vulnerable to the “domino effect”. That is the failure of a single part can incapacitate the whole system. Total reliability identifies the critical parts such that they are designed with the same chance of survivability. In addition, major and minor constraints can also be implemented by a weighing factor Ω [2, 3]. High green energy efficiency η may also be implemented. The general idea is being applied to the design of long-span bridges [9, 10]. Similar applications can be made to the design of tall buildings and power plants. In this respect, sizing of critical components will play a vital role. Put it simply, *the appropriate scale range of damage detection must be known as a priori such that the scheme of total reliability can be applied in design*.

2. Strategy of total reliability

When failure occurs for reasons that were not expected, the structural system is said to be unreliable. The notion of “reliability” was thus borne and connected with the material and/or structural “integrity”. Analytical assessment of these descriptive terms requires specific mathematical representation of the relevant physical parameters. For multifunctional and multi-component systems, there is the added requirement of consistency. A common base for evaluating damage accumulation and energy efficiency would be needed to mitigate ambiguities of the end results. The inability to determine structural integrity degradation in the long run should not be mistaken for the probabilistic character of the physical event. Rather, determination of short term

changes should take precedent. The order of priority can be established by testing the sensitivity of the governing parameters. This additional consideration is necessary for validating the space-time increments chosen in the large scale computations.

2.1. Variance with reliability engineering

Total reliability emphasizes the physical mechanism(s) of structural integrity degradation at the molecular or macroscopic scale. Cumulative damage caused by aging due to changes of the environment, disproportionate time rates of absorbed and dissipated energy, and other effects that limits the life time of the system can be included as additional sub-routines to the overall computational scheme. Short term corrective measures obtained from continuous monitoring of in-situ data enhances the “deterministic” capability of the approach. Probability can be used as a tool in a particular subroutine, but not as the main theme of reliability.

Unlike total reliability, “engineering reliability” regards failure to occur in a black box as a random phenomenon with no information given to the causes of failure. All failure events are assumed to vary with time according to a given *probability density function*. The result is taken to mean that a system has a specified chance of operation without failure before a predicted time. The prediction has no safe guide against changing service conditions, expect that all uncertainties are meshed into the probability function. No commitments are made to the causes and effects of failure. It is too high of a risk to assess life time reliability without any notion of causes and effects.

2.2. Correcting short term prediction from feedback information

Reliability of structural integrity cannot depend on chances even though there are uncertainties involved with the design conditions. Weather prediction cannot depend on chances. Improved satellite surveillance technology, coupled with computer simulation, has improved the reliability of *forecasting* weather prediction. This is equivalent to estimating the reliable operating life of a structural system. The object is to shorten the feedback time for correcting the prediction as design conditions are changed. The state-of

the-art [4, 5] considers 2 to 3 years as the normal predictive capability that accounts for non-equilibrium, non-homogeneity, and intrinsic energy dissipation. Even though, long term aging effects for 12 years or more can be included, the prediction is still based on a fixed set of boundary conditions [6, 7]. Short term corrective measures for prediction is believed to be more reliable provided that feedback from monitored in-situ data are obtainable.

2.3. Blending monitored in-situ data with large scale computational algorithms

Monitored data are often collected from strain gauges attached to the surface while the damage may be hidden in the bulk where the data are needed. The difference between the surface and bulk deserves attention. To begin with, cracks are always initiated from the interior. They become visible by the naked eye only when they penetrate through the surface. This is because the bulk constraint is larger than the surface constraint. The material is less stiff next to the free surface; it becomes stiffer with the distance into the interior as illustrated in Fig. 1(a), which shows the gradual degradation of the stiffness by the changing shade from dark to light as the free surface is approached. This effect was simulated by four homogeneous layered model [11] in Fig. 1(b) for one-half of a finiteness thickness plate from the surface to the mid-plane. Despite the coarseness of the stiffness gradient, it was sufficient to yield a realistic crack growth profile. The crack initiated from the interior where dilatation dominates. It then grew towards the surface where distortion dominates. The shape of the crack depends on the proportion of dilatation to distortion. The constant stiffness model in Fig. 2 would yield an overly higher stress intensity on the surface. This suggests crack initiating from the surface [12] due to the fictitiously high dilatation invoked in the theory that ignores surface effects. Moreover, the results are contrary to the experimental measurements of three-dimensional frozen strain technique.

As in reality, crack initiates from the interior where dilatation dominates. A small, but finite, distance between the surface and the location of fatigue initiated crack for smooth specimens can be found in most text books. This small distance is sufficient change in the distortion-to-dilatation

ratio for initiating a fatigue. Illustrations and explanations of this surface-bulk interaction are no longer uncommon [13, 14]. What should be cautioned is that crack initiation sites are also affected by the quality of the material. Commercial steels are not pristine materials; they may contain pre-existing imperfections in the form of precipitates, inclusions, and layers of delaminated material hidden inside. The strain gauge data in Fig. 3 for crack initiation in contrast to those for pre-existing interior cracks most certainly deserves caution. That is cracks can initiate at locations where gauges were not placed and then propagate internally under the measurement sites for a long distance. Such situations can be mistaken for no crack initiation. On other words, the scenario just mentioned may not be covered by the established laboratory conditions designed only for detecting crack initiation. It is always the unexpected that causes failure. Million dollars worth of computational software and hardware can be in vain if the monitored data are misinterpreted. The alternative would be the *simultaneous detection of crack initiation and compliance* (or stiffness) [8]. This can be accomplished without additional hardware if the depicted criterion is multifunctional in nature.

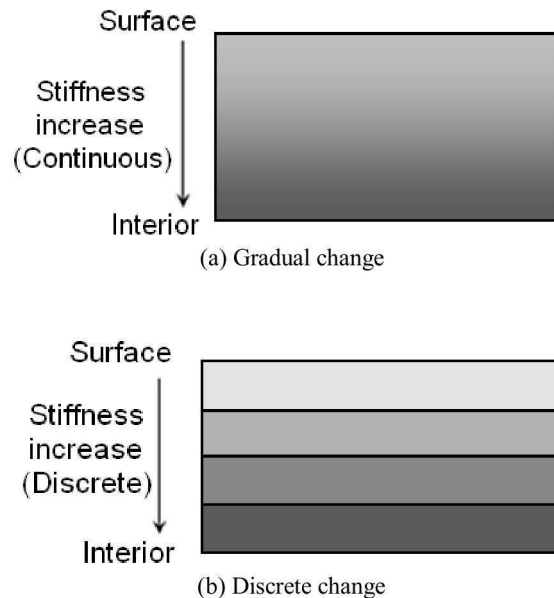


Fig. 1. Physical situation simulated analytically.

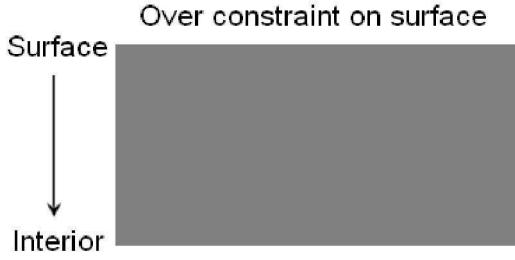


Fig. 2. Surface over constraint for homogeneous stiffness.

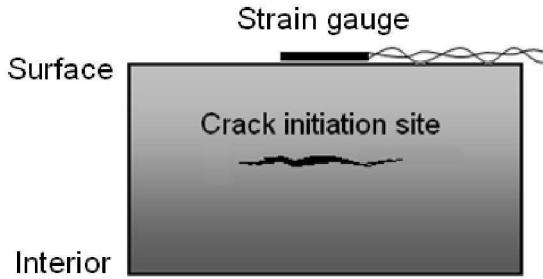


Fig. 3. Crack initiates from pre-existing defects in material.

2.4. Multiscale structural integrity degradation criterion

Ambiguities of end results can be minimized by reducing the redundancies for structural integrity degradation criteria. Instead of using three criteria, one for fatigue crack initiation, one for stable crack growth, and another for the onset of unstable crack propagation, a single SED (strain energy density) criterion serving all three conditions can be used [13]. Crack initiation is assumed to start when the strain energy density function dW/dV reaches the critical value $(dW/dV)_c$ [14] as shown by Eq. (1), which can be used as the material “toughness” with or without pre-existing defects. The crack grows slowly in segments of r_1 , r_2 , etc. until instability when the critical ratio S_c/r_c is reached.

$$\left(\frac{dW}{dV} \right)_c = \frac{S_1}{r_1} = \frac{S_2}{r_2} = \dots = \frac{S_j}{r_j} = \dots = \frac{S_c}{r_c} \quad (1)$$

The depicted analytical model in Fig. 4 coincides precisely with the physical mechanism of crack initiation in polycrystalline materials. As the crack tip rests next to the stronger crystal, voids are initiated at the site of the weaker crystals r_j distance away represented by the first ele-

ment. Additional energy would then be accumulated ahead of the new crack tip until the nearest distance element becomes critical moving the crack tip another segment r_2 . Hence crack growth is a discrete process of connecting the loci of crack initiation points. In this sense, *crack initiation and growth are one of the same physical process*. Experiments suggest that this mechanism remains valid for cracks as small as nanometers in size.

The selection of failure criterion independent of the so referred to “stress-strain analysis” has been taken for granted because of the inability of the classical theories of continuum mechanics to account for damage. Piecemeal repair has caused inconsistencies, and ambiguities that are even more problematic. Space-time rate effects associated with multiscaling have revealed that the changing energy state with material damage disqualifies many of failure or fracture criteria that were previously regarded as the Holy Grail. One of them is $da/dN = C(\Delta K)^n$ based on the use of ΔK for Mode I self-similar crack growth. Fig. 5 shows the sigmoidal curve in the log-log plot for da/dN versus ΔK for the empirical evaluation of C and n . Since ΔK is valid only for the macroscopic crack, and fatigue involves damage accumulation at the microscopic scale, *the proposition of relating da/dN to ΔK for fatigue cracking collapses*. The crack growth rate da/dN involves dual-scale while ΔK is restricted to single scale. This apparent inconsistency has led to numerous discussions in fatigue fracture mechanics of “small cracks” in contrast to large cracks macroscopic in size. References in the open literature are too numerous to be quoted. Most of the arguments are centered on the so-called “threshold region” which is outside the validity of the model, since it is independent of ΔK . When the micro- and macro-effects are connected [15], a straight line can be obtained instead of the sigmoidal curve. It also shows that fatigue crack growth, being mixed at the micro-macro scale, is non self-similar. This, in retrospect, is another reason for invalidating the use of $da/dN = C(\Delta K)^n$. The condition of homogeneous energy release has been invoked because of its relation to the Mode I stress intensity factor. Non-homogeneous energy release can result in negative results [16, 17].

The seemingly innocent use of the mono-scale classical fracture mechanics discipline can go astray when applied to multiscale situations. Returning to Fig. 5, it is seen that the sigmoidal curve can be divided into segments. It so happened that Regions I and II enclose the micro and macro scale transition. The physical crack is unaware of this arbitrary choice of scale division in Fig. 6. The choice could have been combining Regions I and II into a “meso region”. In that case, fatigue crack initiation and growth can be regarded as a single scale process. To compensate for the discontinuity in scaling, a form-invariant scheme [15] can be devised such that the line labeled Region I in Fig. 3 can be rotated clockwise to have the same slope as the line for Region II as indicated in Fig. 7. The line for Region III can also be rotated. All regions would then lie on the same straight line. Results for different scales are then connected to allow scale shifting.

2.5. Multiscale and multi-component systems

Multifunctional systems are multifaceted. They are only as reliable as that for each of the critical component. The means, must therefore, be addressed to associate the system reliability parameters to those for the components. This is accomplished by applying input-output energy flow as shown by the schematic in Fig. 8. The tem Σ contains components enclosed by control volumes Γ , say macro for Σ and micro for Γ . Within each control volume Γ as shown in Fig. 9, still smaller scale components can prevail. Energy loss for the system should be distinguished from energy dissipated for the control volume. The latter is intrinsic while the former is extrinsic which crosses a boundary or interface. The intrinsic energy dissipated is an inherent part of the dual mechanism of contraction and expansion as a result of energy absorption and dissipation. More on this will be discussed in connection with mass pulsation.

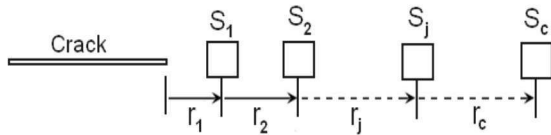


Fig. 4. Crack growth is the loci of crack initiation sites.

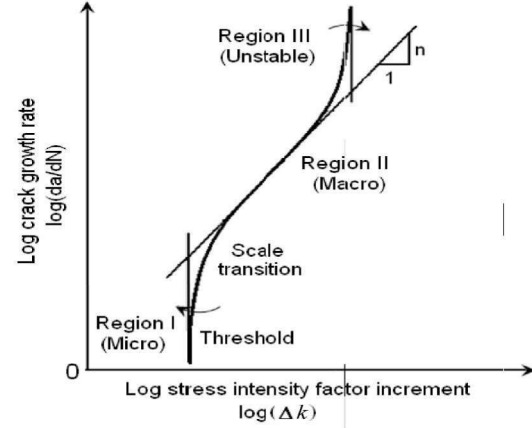


Fig. 5. Traditional two-parameter fatigue crack growth rate.

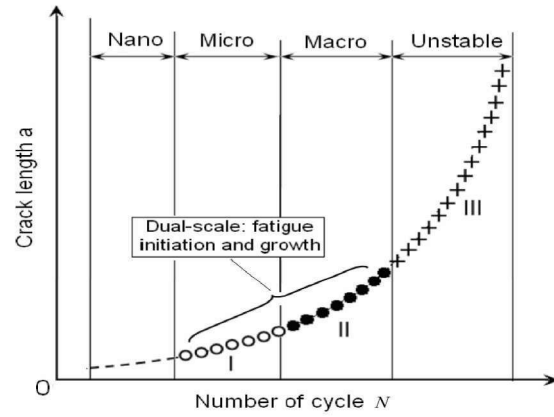


Fig. 6. Multiscale crack growth.

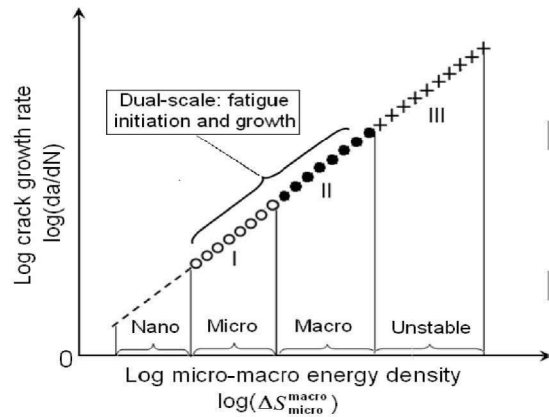


Fig. 7. Form invariant of dual-scale fatigue crack growth rate.

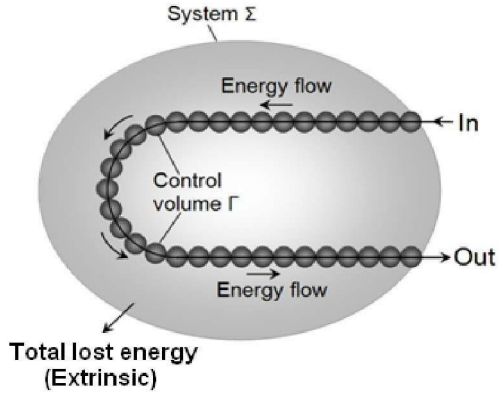


Fig. 8. Energy flow in and out of system and its components.

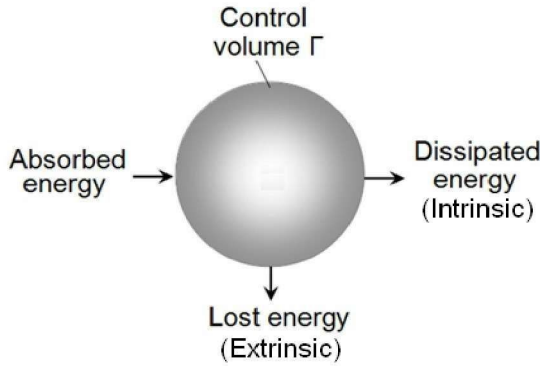


Fig. 9. Control volume characterized by the simultaneity of energy absorption and dissipation.

2.6. Matching space-time rate increments of material damage with simulation

The rate at which energy is transmitted to a specific volume of material determines the extent of damage. Material with different internal structures would absorb and dissipate energy at different rates. These basic characteristics must be observed when simulating the evolution process of material damage by numerical means. That is the size of the elements and the corresponding time increments cannot be chosen independently; they are connected intrinsically and extrinsically. The general scheme [4, 5] for determining these relationships determines the time range of prediction which is inversely proportional to the number of functions that the system has to satisfy.

Numerical or experimental simulation tests are accelerated by shrinking the life time several orders of magnitude in relation to the test time. Fatigue data obtained within a year or less has been

traditionally used to make 100 years life prediction of large structures. This leaves out load sequence effects that are inherent to cumulative damage such as aging. Strictly speaking, only short term prediction is possible. Long term safety can only be assured in short space-time intervals, the reliability of which is a multifaceted consideration.

2.7. Reliability of multifunctional systems

Up to now, reliability has been left undefined. This is a subjective decision that entails risk factors. Let p_1, p_2 , etc. be assigned to reflect the character of the multifunctional system. A multiplicative reliability index R can then be defined as

$$R^m(t) = \int_0^{t_1} \alpha p_1^a dt \int_0^{t_2} \beta p_2^b dt \cdots \int_0^{t_n} \zeta p_n^z dt \quad (2)$$

The weighing parameters α, β , etc. can depend on time while the exponents a, b , etc. are constants. Their evaluation, however, is beyond the scope of this work. The summation reliability index would be

$$R^S(t) = \int_0^{t_1} \alpha p_1^a dt + \int_0^{t_2} \beta p_2^b dt + \cdots + \int_0^{t_n} \zeta p_n^z dt \quad (3)$$

Both Eqs. (2) and (3) include cumulative and sequence effects in time. The $p_1, p_2, \dots, p_j, \dots, p_n$ are related to the *causes and effects* of unreliability. Two classes of reliability can thus be identified:

(1) Weak reliability: The time t_1, t_2 , etc. in any one of the integrals of Eq. (2) is used as the reliability time limit t_f .

(2) Strong reliability: The times t_1, t_2 , etc. in the integrals of Eq. (3) can all correspond to failure in sequence but only one of them is used as the reliability time limit t_f .

Eqs. (2) and (3) can also be used to define the time average R_{ave} and used as a reliability index:

$$R_{ave} = \Sigma R_i(t) / R_{total} \quad (4)$$

In the same way, a multiplicative or summation total reliability index may be written for the system involving the component reliabilities R_1, R_2 , etc. The corresponding forms of Eqs. (2) and (3) for the total reliability of multifunctional systems would be

$$R^m = R_1 R_2 \cdots R_n \quad (5)$$

And

$$R^S = R_1 + R_2 + \cdots + R_n \quad (6)$$

Eq. (5) is a weak condition of total reliability. That is the reliability R_j ($j=1,2,\text{etc.}$) of any single part can directly influence the system as a whole. Note that $R \rightarrow 0$ when $R_j \rightarrow 0$. This is not true for the stronger condition in Eq. (6), where R_j may vanish individually while R would be reduced only by the vanishing part. A combination of Eqs. (4) and (5) can also be formulated with added sophistication. The major emphases, however, should be placed on rapid feedback of monitored in-situ data for corrective measures. Since $p_1, p_2, \text{etc.}$ will change in time, $R_1, R_2, \text{etc.}$ will also change accordingly. Time average R_{ave} for Eqs. (5) and (6) can also be found. The choice of using Eqs. (2) to (6) or their combinations is application specific. An example of the causes and effects of unreliability may be illustrated by letting, say $p_1, p_2, \text{and } p_3$. They can correspond to the critical energy density function $(dW/dV)_c$, energy efficiency η , and life expectancy, expressed in total fatigue cycles ΣN_i , respectively. Remember that of $p_1, p_2, \text{and } p_3$ is a function of time. Complexity of total reliability will rise with the increase number of causes and effects of unreliability.

3. Molecular structure systems

An intrinsic mechanism for energy dissipation is postulated such that the definition can hold independent of the body size at large. Recent measurement of “Micropulsations” [18] associated with electromagnetic fields in space seem to suggest that a basic mechanism for dissipation energy. This notion is not unrelated to the CTM/IDM [19, 20] mass pulsation model. The singular crack tip was postulated to absorb-dissipate energy in unionism as a pulse that is intrinsic to any materials. This is distinguished from the extrinsic energy loss crossing a boundary or interface of any physical systems at large.

3.1. Rule of the thumb

Following the simple minded concept of the CO₂-to-O₂ approach, a mathematical statement for the energy efficiency can be made:

$$\eta = \left(1 - \frac{\mathcal{D}}{\mathcal{A}}\right) = \left(1 - \frac{CO_2}{O_2}\right) \quad (7)$$

For cities that are heavily infested with heavy smog, a 0.75:1 ratio for CO₂-to-O₂ would yield an energy efficiency $\eta=25\%$. A very optimistic ratio would be 0.45:1 for CO₂-to-O₂ with an energy efficiency of $\eta=50\%$. A realistic and verifiable target for CO₂/O₂ ratio reduction within the next 10 years [1, 3] should be about 22%.

3.2. Open system kinetic molecular theory

Energy dissipation of small bodies is an issue that even quantum mechanics chooses to ignore. Without an estimate of \mathcal{D} , it would not be possible to address the efficiency of molecular structures. A refinement of Eq. (7) needs to be made:

$$\eta = \left(1 - \frac{\mathcal{D}}{\mathcal{A}}\right) = \left(1 - \frac{\mathcal{M}_{CO_2} \mathcal{V}_{CO_2}^2}{\mathcal{M}_{O_2} \mathcal{V}_{O_2}^2}\right) \quad (8)$$

Eq. (8) was derived by using the following relations

$$\begin{aligned} 2\mathcal{A} &= \mathcal{M}_{O_2} \mathcal{V}_{O_2}^2 \\ \text{and} \\ 2\mathcal{D} &= \mathcal{M}_{CO_2} \mathcal{V}_{CO_2}^2 \end{aligned} \quad (9)$$

Calculation of Eq. (8) or Eq. (9) is straightforward since the properties for non-ideal gases in open system can be found in [18, 19]. A weighing factor Ω can also be inserted into Eq. (8) to yield

$$\eta = \left(1 - \frac{\mathcal{D}}{\Omega \mathcal{A}}\right) = \left(1 - \frac{\mathcal{M}_{CO_2} \mathcal{V}_{CO_2}^2}{\Omega \mathcal{M}_{O_2} \mathcal{V}_{O_2}^2}\right) \quad (10)$$

The possibilities of having $\Omega < 1$ or $\Omega > 1$ provides the means to account for environmental effects that can increase or decrease the system efficiency. Upper and lower bounds of the efficiency

index η can thus be established for molecular systems with $33\% < \eta < 67\%$.

3.3. Mass pulsation model

It should be said in passing that truly non-equilibrium and non-homogeneous systems cannot assume the energy dissipation to be known. It must be determined as a function of time in relation to the absorbed energy. Energy dissipation is not only time rate sensitive, it also depends on the time rate of energy absorption, both of which are implicit by nature. Their assessments have led to the notion of mass pulsation [19, 20] requiring a knowledge of the total system behavior for matching the time rates of energy absorption in relation to those of dissipation at the different size-time scales. This is equivalent to choosing the number of slices for the space and time increments in the numerical calculations. In this way, the energy index η can be expressed as

$$\eta = \left(1 - \frac{\mathcal{M}_{\downarrow}^{\downarrow}}{\Omega \mathcal{M}_{\downarrow}} \right) \quad (11)$$

Eq. (10) involves both the mass of absorption \mathcal{M}_{\downarrow} and mass of dissipation $\mathcal{M}_{\downarrow}^{\downarrow}$, which are distinguished, respectively, by the subscript arrow and superscript arrow. Both arrows are pointing downward indicating that they are decreasing functions of time. The notations are chosen specifically to reflect the between \mathcal{M}_{\downarrow} and $\mathcal{M}_{\downarrow}^{\downarrow}$. Refer to Fig. 10 for a physical interpretation of mass pulsation. The crack tip has been shown in [20] to play a unique role in energy absorption and dissipation. When energy is pumped into a cracked region, it tends to be packed with increasing strength at the crack tip until a threshold is reached. The energy flow will then reverse its direction, as if there exists an intrinsic energy limiting reservoir such that the energy would over flow once the reservoir is full. The in-flow and out-flow of energy give rise to contraction and expansion of the crack tip region locally that is displayed, respectively, in Figs. 10(a) and 10(b). After the crack tip establishes a new position, the dual mechanism of energy absorption-dissipation repeats again. Irreversible damage of material is thus said to occur by “mass pulsation”. The pulse

interval depends on the rate of energy input and adopts a unique pattern for a given material internal structure.

3.4. Time dependency of efficiency

The efficiency $\eta(t)$ in Eq. (11) is time dependent [4,5]. Keep in mind that both \mathcal{M}_{\downarrow} and $\mathcal{M}_{\downarrow}^{\downarrow}$ vary with time. Efficiencies for different time segments $\eta_i(t)$ may be averaged to give

$$\eta_{ave} = \sum \eta_i(t) / \eta_{total} \quad (12)$$

Moreover, $i=1,2,\text{etc.}$ may represent different molecular structures. In this case, Eq. (12) would yield the average of a heterogeneous molecular system. In general, the efficiency is a function of time:

$$\eta(t) = \int_0^t \eta_i(t) dt \quad (13)$$

The definition of $\eta(t)$ based on \mathcal{D} and \mathcal{A} applies to molecules and structural systems.

4. Large structural systems

The efficiencies of large structures can be best estimated by considering the useful energy against that wasted at the macroscopic scale. The difference between the input and output energy can be interpreted in terms of \mathcal{D} and \mathcal{A} as given by

$$\eta = \frac{\Omega \mathcal{A} - \mathcal{D}}{\Omega \mathcal{A}} \quad (14)$$

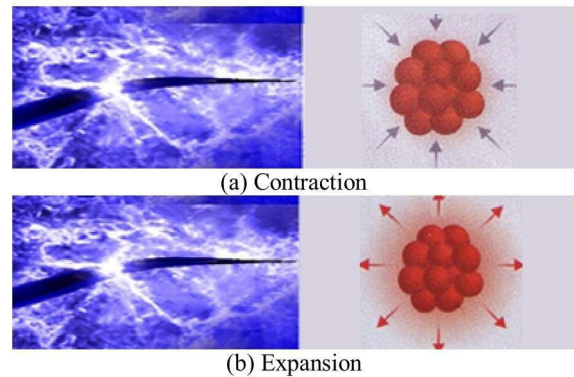


Fig. 10. Energy absorption and dissipation at crack tip [20].

Even though the general appearance of Eq. (14) for large structures is similar to Eq. (7) for molecules, the details of findings \mathcal{D} and \mathcal{A} will differ.

4.1. Selection of weighing factor Ω

Fig. 11 shows graphically the beneficial and detrimental effects of the environment referenced to $\Omega < 1$ or $\Omega > 1$, respectively. Plotted are the ratio \mathcal{D}/\mathcal{A} versus η . Note from Eq. (11) that higher efficiency corresponds to the relative magnitude of \mathcal{D} to \mathcal{A} and hence the ratio \mathcal{D}/\mathcal{A} . The regions $\Omega < 1$ and $\Omega > 1$ are separated apart by the straight line $\Omega = 1$. The factor Ω provides the means to account for environmental effects that can increase or decrease the system efficiency. The selection of Ω relies on experience. Maintenance record of building and air transport can be useful for assigning values for the weighing factor. From the air transport industry, the following scenarios can be used:

More than average loss of energy corresponds to $\Omega > 1$:

- (1) Bad weather conditions can consume additional fuel, Fig. 12(a), .
- (2) Congested air traffic entails longer period of taxing on runway, Fig. 12(b).

Less than average loss of energy corresponds to $\Omega < 1$:

- (1) Longer flight routes with less take-offs.
- (2) Favorable weather conditions.

Similar considerations can be used for buildings.

Unfavorable conditions: $\Omega > 1$ applies to ordinary buildings.

- (1) Under insulation, energy leaking windows and doors.
- (2) Over heating, under cooling and deficient water systems.

Favorable conditions: $\Omega < 1$ applies to intelligent buildings.

- (1) Occupancy sensors and timers to save energy.
- (2) Improved air and water handling systems to mitigate over heated and under chilled water.

Tall buildings are source of large energy consumptions. Fig. 13(a) shows an ordinary building that may consume less energy than the skyscraper because it has less floor space, but it is much less efficient. The skyscraper in Fig. 13(b) consumes

more total energy but it dissipate less relative basis making the process more energy efficient. To reiterate, it is the ratio \mathcal{D}/\mathcal{A} that counts.

4.2. Air transport payload efficiency

The concept of payload will be used to determine the efficiency of large structural systems. Efficiency in transportation is determined by the energy used to carry certain load from one destination to another. Vehicle with the least weight carrying the largest load would be most efficient. This can be expressed by the relation

$$\eta = \frac{\text{Full load} - \text{Empty load}}{\text{Full load}} \times 100\% \quad (15)$$

The efficiency of the vintage Boeing 757-200 of the 1980s in Fig. 13(a) can be computed as

$$\eta = \frac{(80,520\text{kg}) - (57840\text{kg})}{(80,520\text{kg})} \times 100\% = 28\% \quad (16)$$

It is constructed from metal alloys having a relatively low strength-to-weight ratio in comparison to composites. The Boeing 787-9 of the 2010s using composite materials with a high strength-to-weight ratio has a much higher efficiency of being

$$\eta = \frac{(24.49 \times 10^4 \text{kg}) - (11,52 \times 10^4 \text{kg})}{(24.49 \times 10^4 \text{kg})} \times 100\% = 52.96\% \quad (17)$$

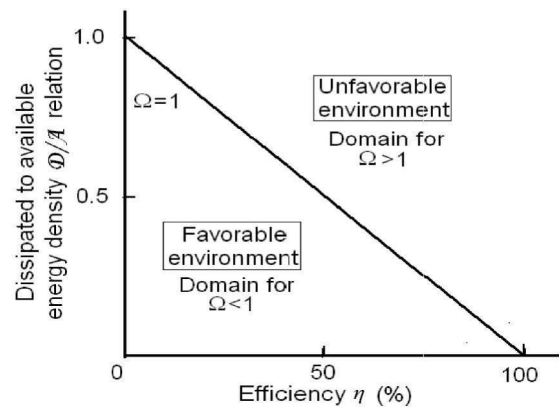


Fig. 11. Domain of efficiency for $\Omega < 1$ or $\Omega > 1$.